wind

MDPI

Article

Comparison of S-N Curves from International Fatigue Design Standards for a Better Understanding of the Long-Term Operation of Offshore Wind Turbine Welded Foundations

Federico Della Santa [1], Gianluca Zorzi [2] and Ali Mehmanparast [1,*]

[1] Department of Naval Architecture, Ocean and Marine Engineering, University of Strathclyde, Glasgow G1 1XQ, UK; federico.della-santa@strath.ac.uk
[2] RWE Offshore Wind GmbH, Hamburg 20354, Germany
* Correspondence: ali.mehmanparast@strath.ac.uk

Abstract: Fatigue poses significant challenges for the structural integrity of monopiles, the most common type of foundation for offshore wind turbines. These structures are usually manufactured by rolling and welding together large steel plates. Offshore wind turbines are typically designed to operate for 20 years or longer, thus the number of cycles to failure (N_f) that these structures are required to withstand lies in the so called ultrahigh-cycle fatigue (UHCF) regime ($N_f > 10^8$). Moreover, because, in the past few years, there has been a continuous increase in the size of monopiles, the fatigue life reduction caused by the utilization of thicker steel plates plays an important role (i.e., thickness or size effect). Different regions worldwide apply distinct codes to ensure that offshore structures can withstand fatigue damages, but most of them are tailored for the high-cycle fatigue (HCF) regime. This paper seeks to compare a selection of these codes, highlighting both differences and similarities, while also questioning their suitability in the UHCF regime and for much thicker structures (compared to the reference thickness values reported in the standards). By doing so, it aims to contribute to the ongoing efforts to optimize the efficiency of the fatigue life assessment of offshore wind infrastructures. The focus of this study is on double-V transverse butt welds and their S-N curves in air and seawater (with and without cathodic protection), while the analyzed standards are those provided by the Det Norske Veritas (DNV-RP-C203-2021), the British Standards Institution (BS 7608, including the amendments of 2015), and the European Union (EN 1993-1-9, updated in 2005). The results have been discussed in terms of the level of conservatism that each of these standards offers and in identifying the areas for further research to enable extended lives in the current and future offshore wind monopile foundations.

Keywords: fatigue design; offshore wind turbine; monopile; ultrahigh-cycle fatigue; thickness effect

Citation: Della Santa, F.; Zorzi, G.; Mehmanparast, A. Comparison of S-N Curves from International Fatigue Design Standards for a Better Understanding of the Long-Term Operation of Offshore Wind Turbine Welded Foundations. *Wind* **2024**, *4*, 251–274. https://doi.org/10.3390/wind4030013

Academic Editor: Francesco Castellani

Received: 17 July 2024
Revised: 12 September 2024
Accepted: 18 September 2024
Published: 21 September 2024

1. Introduction

With the increasing interest in electricity production from clean energy sources as a significant step towards national and international targets to achieve Net Zero, offshore wind has experienced exponential growth in the past two decades and is anticipated to continue its rapid expansion around the world in the years ahead. In a recent report by the International Renewable Energy Agency (IRENA), it has been shown that, in order to achieve the restriction of temperature rise below 1.5 °C, following the Paris agreement at the UN Climate Change Conference (COP21) in 2015, a significant growth in energy production using a wide range of renewable energy sources would be required by 2030 and beyond [1]. Among all renewable energy sources considered in [1], offshore wind has been found to have great potential for combating climate change; therefore, it has been recommended to adopt necessary strategies to boost its installed capacity. Considering that the current offshore wind turbines are typically designed for 20–25 years of operation, with slightly longer design lives in recent projects, it is important to develop strong engineering

knowledge of the long-term design and integrity assessment in order to be able to meet the initial design lives without any premature failures in the first instance and to subsequently consider extending the life of the aged wind turbines beyond the initial design life. In fact, life extension not only contributes to electricity production for extended durations, but also reduces the levelized cost of energy (LCoE) for offshore wind by increasing the lifespan in conjunction with the optimization of inspection and frequency of repair operations.

Offshore wind turbines consist of three main parts: (i) the foundation, which supports the entire structure and tolerates the weight of the wind turbine structure; (ii) the transition piece, which connects the foundation to the tower; and (iii) the tower, at the top of which the rotor and nacelle are installed. In some of the new designs, innovative attempts have been made to remove the transition piece from the structure and directly connect the foundation to the tower. Among these three main parts, the foundation, which is located under the sea level and connects the structure to the seabed, is the most critical, with significant allocated costs associated with its manufacturing, transportation, installation, and inspection [2]. The type of offshore wind turbine foundation is selected based on the water depth, the soil condition, and the distance from the shore. Overall, it can be in the form of a fixed-bottom structure for shallow waters or a floating structure for deeper waters. Knowing that the majority of existing offshore wind turbines are installed in relatively shallow waters, the number of fixed-bottom structures is significantly higher than that of floating foundations at the moment.

The most common type of offshore wind turbine foundation that is predominantly used to support the existing offshore wind turbines around the world is monopile [3]. The main steps in the fabrication of offshore wind turbine monopile foundations include the following: (i) the application of the cold rolling and bending process to transform the high-thickness structural steel plates into a circular shape; (ii) the longitudinal welding of the ending edges to produce individual cylinders, which are often referred to as cans; and (iii) the circumferential welding of the cylinders to reach the required length for the designed monopile [2]. Monopiles are presumably one of the largest types of energy structures, and they can have a length of up to 120 m and a wall thickness of 150 mm [4]. While welds are introduced in both axial and circumferential directions during the fabrication of monopiles, the circumferential welds are the most likely to fail, due to the loading conditions during operational phases. The monopile design considers the bending moments generated by wind and waves, which create longitudinal stresses acting perpendicular to the circumferential welds, making them a critical spot. All welds are conducted both inside and outside of the monopile using a double-V groove multi-pass butt weld strategy, which is appropriate for very thick structures such as monopiles.

Welding is a broadly used joining technique, but the fatigue resistance of a welded joint is usually lower than that of the parent material, due to the introduction of defects and residual stresses [5,6]. Fatigue is the dominant degradation mechanism, which results in damage or failure in the presence of cyclic loads. Under this condition, components may start to crack when the maximum stress is well below the yield stress or ultimate tensile strength of the material [7]. Since fatigue cracks in the as-welded condition usually initiate at the weld toes where a stress concentration factor is present [8] and welding defects can contribute to the initiation and propagation of cracks [9], fatigue becomes a significant failure mechanism in welded structures, which would heavily depend on the welding quality and the extent of defects. Thus, careful considerations must be made in the short- and long-term fatigue design of offshore wind turbine monopiles that would operate for an extended number of years in aggressive offshore environments, where cyclic loads are constantly applied on the welded structure due to the exertion of wave, wind, and current forces.

To design monopiles against fatigue for a desired lifetime, there are several international standards that are available and are commonly used by designers in the offshore wind industry. In this work, the fatigue design guidelines and recommendations in three of the main international standards, which are widely used for welded structures, have been

thoroughly analyzed to identify the knowledge gaps for the long-term structural integrity assessment of monopiles. The standards considered in this study are DNV-RP-C203-2021 (DNV) by Det Norske Veritas [10], BS 7608:2014 + A1:2015 (BS) by the British Standards Institution [11], and EN 1993-1-9:2005:E (EC) by the European Union [12]. These standards have been comprehensively investigated with respect to double-V butt welds by considering the recommended S-N fatigue curves for different environments and thicknesses. As a result of the extensive examination of the standards, the knowledge gaps for the operation of aged offshore wind turbine foundations have been identified and discussed in light of the essential research that needs to be conducted in the future to confidently operate these high-value assets until the end of the initial design life and further consider the residual life remaining in the welded monopiles at the end of the initial design life to enable life extension.

2. Basic Fatigue Principles for the Design of Welded Structures

In order to characterize the fatigue behavior of engineering materials under the force control mode, cyclic tests are performed on several specimens by periodically varying the load between an upper and a lower limit, which eventually leads to a maximum (σ_{max}) and minimum (σ_{min}) internal stress, respectively. In fatigue tests, the stress range can be defined as the difference between the maximum and minimum stress $\Delta\sigma = \sigma_{max} - \sigma_{min}$, while the mean stress is defined as the average of these two values $\sigma_m = (\sigma_{max} + \sigma_{min})/2$.

The results from fatigue tests under uniaxial loading condition are often presented by plotting the stress range $\Delta\sigma$ (commonly referred to as S) against the number of cycles to failure (N_f) in log–log coordinates. The data are then fitted using a power-law equation to obtain the so-called S-N (stress versus number of cycles to failure) curves and, when log–log axes are employed, these fit lines appear straight.

Fatigue tests in air are typically performed using servo-hydraulic machines, which usually operate within a frequency range of 1–10 Hz [13]. This parameter can be significantly increased using resonance [14] or ultrasonic fatigue machines [15], thus accelerating experiments and mitigating the time-consuming nature of fatigue testing. However, because of the contribution of the time-dependent corrosion damage to the fatigue failure mechanism, this approach is not suitable for corrosion–fatigue tests [7,16]. To address this aspect, international standards often provide different S-N curves depending on the environment, specifically for the offshore structure design for air, seawater with cathodic protection, and seawater under free-corrosion conditions.

While characterizing the long-term fatigue behavior of aged offshore wind turbine foundations, it is of great importance to employ adequate levels of conservatism and accurate thickness correction factors. These two aspects are further elaborated and explained in the following two sections.

2.1. Introduction to the Ultrahigh-Cycle Fatigue

For some materials, below a specific stress range, there is no failure observed during fatigue tests under constant amplitude loading conditions. This threshold is usually referred to as the fatigue limit (FL) or the endurance limit, and, in the S-N curve, it is illustrated as a horizontal line, as shown in Figure 1a. This leads to the assumption that, for stress ranges lower than the FL, the corresponding number of cycles to failure would be infinite under constant amplitude loading conditions [13]. Since this parameter is defined as a stress range, it is measured in MPa [7]. However, the concept of fatigue limit has to be treated carefully, especially under variable amplitude loading conditions and/or in the free-corrosion environment. Assuming that a frequency of 10 Hz is employed during a typical fatigue test in air, it will take 12–116 days to reach 10^7–10^8 cycles. Therefore, S-N fatigue tests often start with a relatively high stress range, and, in subsequent tests, the stress range is gradually reduced by considering the option to interrupt the experiment if the specimen does not fail for a significantly high number of cycles. When this happens, the data point is reported as a run-out. Also, fatigue data are subjected to higher scatter in

the long-life fatigue region (i.e., UHCF region) than in the short-life fatigue region. In other words, the lower the stress range, the higher the scatter [17].

Given that testing the material under frequencies of less than 10 Hz using servo-hydraulic machines would be very time consuming, particularly at low stress range values, there is an essential need to consider more advanced test methods to facilitate the investigation of the long-term fatigue behavior of the material, for instance, when in air, by increasing the frequency at which the fatigue test is carried out.

In 1999, Bathias used a piezoelectric fatigue machine to show that, after 10^7 cycles, fatigue failure can still take place in several alloys [18]. Thus, without enough experimental data, an infinite fatigue life cannot be guaranteed. Moreover, during the failure analysis of his specimens, he observed that cracks originate at the surface for high $\Delta\sigma$ and low N_f and in the bulk for low $\Delta\sigma$ and high N_f (where high and low depend on the alloy and the test conditions). These observations from this study and other similar studies introduced the concepts of high-cycle fatigue (HCF) and ultrahigh-cycle fatigue (UHCF) regimes. Nevertheless, there is a lack of distinct demarcation between the HCF regime and the UHCF regime based on the number of cycles to failure. The HCF regime conventionally stops around 10^6–10^7 cycles, while UHCF lies between 10^8 and 10^{11} cycles [13].

In the past few years, the fatigue behavior of materials in the UHCF regime have been investigated using accelerated testing techniques. While certain materials exhibit a discernible fatigue limit, even within the UHCF regime (as depicted in Figure 1a), others, such as some aluminum alloys, demonstrate an absence of a fatigue limit in the high-cycle region (refer to Figure 1b). Additionally, there are materials, such as JIS SUJ2 steel (a high-carbon chromium steel for bearing use [19]), that exhibit two fatigue limits (as schematically shown in Figure 1c) [20].

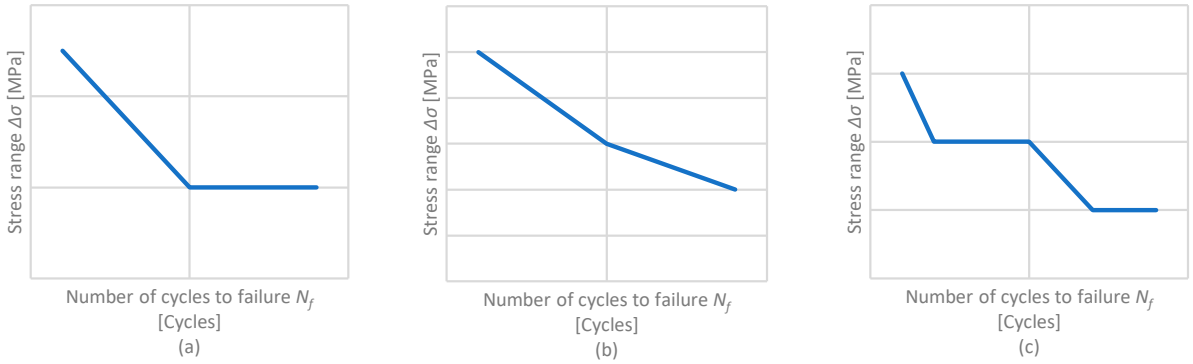

Figure 1. Log–log S-N curves representing various fatigue behaviors with (**a**) one fatigue limit, (**b**) no fatigue limit, and (**c**) two fatigue limits (adopted from [20] and reproduced for the current study).

2.2. Introduction to the Thickness Effect

Another key feature of fatigue is related to what is generally referred to as the thickness effect. In simple terms, it can be described by stating that the greater the thickness of the specimen (or the diameter, depending on the shape), the lower the fatigue life. This phenomenon is attributed to the increased probability of defects in the material, and it was first investigated by Weibull in 1938 [21,22]. In his publications, he referred to "weak places" to describe flaws that diminish the strength of the material. Eventually, once the number of weak places per unit volume is fixed, the probability of rupture increases with the volume. This approach is connected to the concept of the weakest link. An interesting application of this theory was provided by the same author in 1951 to describe the fatigue life frequency curve (number of specimens versus number of cycles to failure) of a carbon steel [23].

Other reasons that underlie the thickness effect are the stress gradient effect and the geometric effect. The former explains the longer fatigue lives of thin sections under bending [24], while the latter has been investigated by Berge in 1985 and predicts an increment in the stress concentration at a weld toe while decreasing the ratio ρ/t (notch root

radius at the weld toe over the thickness of the plate) [25]. Another important observation reported by Berge is that ρ is mostly affected by the last pass at the weld toe and not by the thickness of the plate.

3. International Standards for Fatigue Design of Welded Structures

The DNV and BS standards share the same formulation to describe the fatigue behavior of welded joints using a linear correlation between N_f and $\Delta\sigma$ in log–log axes (i.e., a power-law correlation in normal scale), which appears as a straight line. This formula, in the general form, can be written as shown in (1).

$$\log N_f = q - m \log \Delta\sigma \tag{1}$$

In this equation, both the intercept q and the inverse slope m are positive numbers, and their values depend on the chosen standard, the class of the welded joint, the environment, and the value of N_f. These two parameters are dimensionless, while $\Delta\sigma$ is expressed in MPa and N_f in cycles. It is worth noting that the S-N equation in the standards reports $\log N_f$ as the dependent variable, therefore, it would be reasonable to find it on the Y-axis; however, for the ease of use in industry, S-N curves are conventionally presented with this parameter along the X-axis.

The EC standard employs the same power-law correlation between N_f and $\Delta\sigma$, but presents a different formula to calculate fatigue lives. This is reported in (2), as follows:

$$\begin{gathered} \Delta\sigma^m N_f = \Delta\sigma_{EC}^m \cdot 2 \cdot 10^6 \text{ for } N_f \leq 5 \cdot 10^6 \\ \Delta\sigma^m N_f = \Delta\sigma_{EC,2}^m \cdot 5 \cdot 10^6 \text{ for } 5 \cdot 10^6 \leq N_f \leq 10^8 \\ \Delta\sigma_{EC,2} = \left(\tfrac{2}{5}\right)^{1/3} \Delta\sigma_{EC} \end{gathered} \tag{2}$$

where $\Delta\sigma_{EC}$ and $\Delta\sigma_{EC,2}$ represent the stress range at two and five million cycles, respectively. It can be seen that this mathematical power-law formulation is the same as the one reported in BS and DNV. However, for the ease of presentation and comparison, the results from EC in the rest of the paper are converted from the EC format and presented in the form of (1) (i.e., by means of the parameters q and m instead of $\Delta\sigma_{EC}$ and $\Delta\sigma_{EC,2}$).

Other useful parameters are the location of the change in the inverse slope (CS), given in cycles, and the fatigue limit (FL), given in MPa (see Figure 2). As already mentioned in Section 2.1, the S-N curves might display none, both of them, or even two of each. It is also worth noting that, in the standards considered in this study, no recommended S-N curves can be found to exhibit fatigue behavior in the form of that shown in Figure 1c.

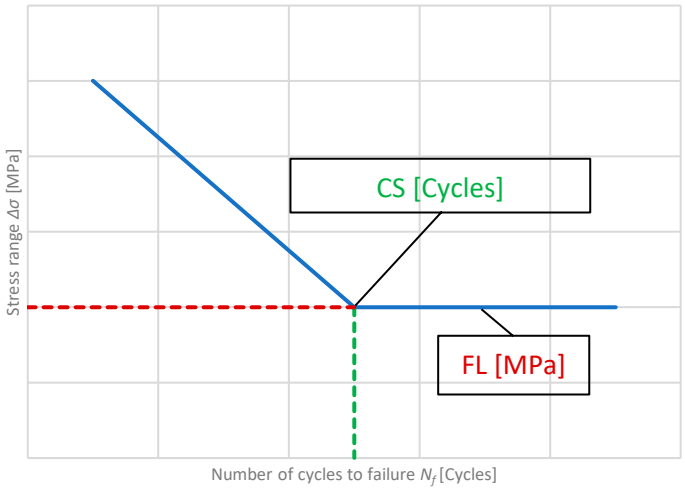

Figure 2. Schematic illustration of S-N curve showing the positions of the CS and FL.

3.1. Conditions of Interest

In this section, the conditions under which the analysis included in this work has been carried out are summarized. The reason behind their selection is driven by the common practice during the fabrication and operation of offshore wind monopile foundations.

The material that is commonly used in the manufacturing of offshore wind turbine foundations is S355 structural steel [26,27]; however, it is worth noting that the recommended S-N design curves provided in the standards are derived from test data on a wider range of steels that are employed in various industries. Additionally, due to the high thickness of the offshore wind monopile foundations, double-V butt welds are often implemented in the fabrication process.

The environments under investigation in this study are air, seawater with cathodic protection, and seawater under free-corrosion conditions. While BS and DNV provide fatigue design curves for all three of these operational environments, the EC standard does not cover the effect of a seawater environment and only presents the S-N design curves in air.

In the DNV standard, the fatigue test data were generated using a constant load ratio $R = \sigma_{min}/\sigma_{max}$ of zero. For welded connections without significant residual stresses, a correction factor f_m is provided to account for other values of R using (3), as follows:

$$f_m = \frac{\sigma_t + 0.8|\sigma_c|}{\sigma_t + |\sigma_c|} \tag{3}$$

where σ_t and σ_c are the maximum tensile and the compressive stress, respectively, and f_m multiplies $\Delta\sigma$ in (1). On the other hand, in the BS standard, the effect of the load ratio (hence mean stress) is not taken into account, and no modification factor is proposed to adjust the curves based on the load ratio.

Another important observation is that, for stress-relieved welded joints without any significant residual stresses, the EC standard suggests increasing the stress range at two million cycles when a part of the cycle is in compression. The formula provided by this standard is reported in (4).

$$\Delta\sigma_{EC} = |\sigma_{max}| + 0.6|\sigma_{min}| \tag{4}$$

It is also worth noting that the frequency and temperature are specified only in BS for a seawater environment, with the intention to replicate North Sea conditions (i.e., frequency between 0.15 and 0.5 Hz and temperature between 5 and 20 °C). As regards the loading condition, the focus of this study is on the S-N curves derived from the case of constant amplitude. No bending has been considered.

To obtain useful S-N curves to employ in fatigue design, standards recommend to lower the mean fit made to the data by two standard deviations (SD) calculated for $\log N_f$. The values of q reported in the following sections for DNV and BS are already associated with the mean-2SD, which provides a 97.7% probability of survival. While, in these two standards, there are formulae that allow us to tune this parameter for different welding conditions, in EC, the value of the stress range at two million cycles for each structural detail is fixed and was calculated for a 75% confidence level of 95% probability of survival for $\log N_f$.

3.2. Classification of Welds

Following the classification of structural details, the analyzed classes of interest for offshore wind monopile applications are C1 and D, according to the DNV standard; C and D, according to the BS standard; and 112 and 90, according to the EC standard. All of these classes refer to double-V groove transverse butt welds. Among them, C1, C, and 112 generally represent high-quality ground flush (GF) welds, whereas D and 90 represent welded joints under as-welded (AW) conditions, meaning that there is no weld toe grinding. The latter is often implemented in the design and fabrication of offshore wind monopiles due to time and cost savings [26]. Both types of welds are reported in Figure 3; in addition,

for AW conditions, the parameters h (height of the weld convexity), l (length of the weld seam), and ρ (weld toe radius) are also given. It is also worth mentioning that class C from the DNV standard is suitable for ground flush welds, however, class C1, which is slightly more conservative, remains the preferred one for the fatigue design of offshore wind turbine monopiles.

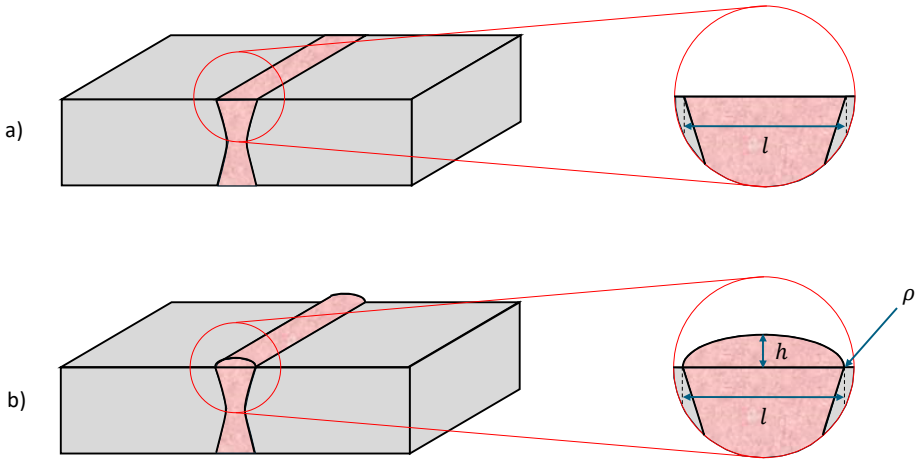

Figure 3. Difference between (**a**) ground flush and (**b**) as-welded conditions. The parameters h (height of the weld convexity), l (length of the weld seam), and ρ (weld toe radius) are reported.

A comprehensive description of the double-V groove butt welded joints considered and investigated in the present study is summarized in Table 1, along with the corresponding classes. The column titled "Type of weld" reports whether the class refers to a ground flush (GF) or an as-welded (AW) joint, while the column titled "Allowed elevation" reports whether there are some restrictions on potential changes in the width or thickness. The formula for width and thickness elevation is shown in (5), as follows:

$$width\ elevation = \frac{a_w}{b_w}\ thickness\ elevation = \frac{a_t}{b_t} \tag{5}$$

where a_w, a_t, b_w, and b_t are the legs of the rectangular triangle drawn on the slope that connects the two welded plates when differences in the width or thickness are present. All of these parameters can be seen in Figure 4.

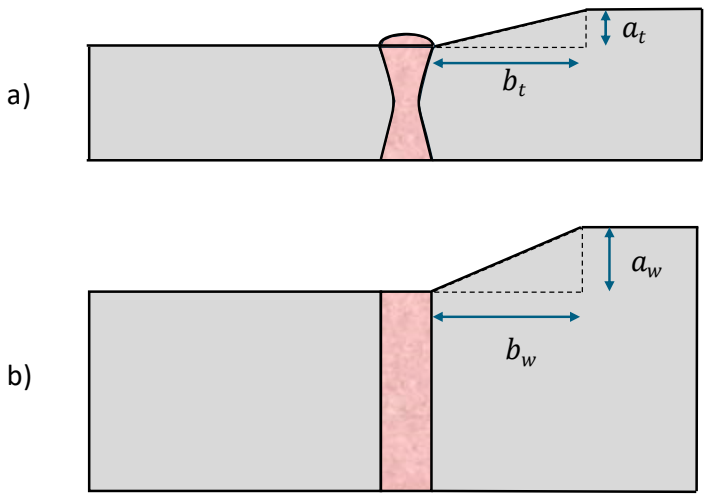

Figure 4. Explanation of the elevation by means of an as-welded joint seen from both a (**a**) side and (**b**) top view.

Table 1. Weld classifications for double-V transverse butt welds taken from DNV, BS, and EC.

Standard	Class Name	Type of Weld	Allowed Height of Convexity	Allowed Elevation	Notes	Ref.
DNV	C1	GF	$h = 0$	<0.25	Specific acceptance criteria and NDT are required for a weld to belong to this class.	Table A-5 in DNV [10]
	D	AW	$h < 0.1\ l$	<0.25		
BS	C	GF	$h = 0$	Not allowed	It is reported that this class should not be employed for structural purposes.	Table 5 in BS [11]
	D	AW	Not reported	<0.25		
EC	112	GF	$h = 0$	<0.25	NDT are required, but it is not specified which ones. No S-N curves in seawater.	Table 8.3 in EC [12]
	90	AW	$h < 0.1\ l$	<0.25	NDT are required, but it is not specified which ones. No S-N curves in seawater.	

In double-V groove transverse butt welds under tension fatigue, cracks are expected to initiate at the weld toe for the AW condition, where a stress concentration factor can be calculated, and near the heat-affected zone (HAZ) for GF welds, where material mismatch, change in local properties, and grain size variation take place. Under cyclic tensile loading conditions, cracks will initiate at the outer surface or at internal defects in the case of GF welds and grow through the thickness of the welded plate.

Depending on the standard and on the class, various non-destructive tests (NDT) and weld quality acceptance criteria may be required. To account for them, DNV refers to other documents, BS provides a thorough table, and EC mentions that some NDT would be required, without any further specifications.

3.3. S-N Fatigue Design Curves from Various Standards

In this section, the S-N curves for classes C1 and D from DNV, C and D from BS, and 112 and 90 from EC are presented in air, seawater with cathodic protection, and seawater under free-corrosion conditions. The main features of the design curves are highlighted as a first step towards the final comparison between the three standards.

In Figure 5, the design curves from DNV for classes C1 and D are plotted for all three environments. As seen in this figure, under cathodic protection conditions, the change in the inverse slope occurs at $N_f = 10^6$, an order of magnitude earlier than the air condition (where it takes place at $N_f = 10^7$). On the other side, the value of the inverse slope m is the same for both conditions (three before the CS and five after). Notably, for $N_f > 10^7$, the two curves overlap, indicating that, with a stress range low enough to reach the UHCF region, there is no difference between the seawater with cathodic protection and air conditions. Moreover, it can be seen that, in DNV, there is no change in the inverse slope for the free-corrosion environment. Same considerations can also be made for class C1.

It is important to remember that, while an FL might be achieved under constant amplitude fatigue loading conditions, it usually does not occur under variable amplitude conditions, which are typical for offshore structures. Therefore, DNV recommends an inverse slope of five in the UHCF region. Moreover, for the welded connections considered in this study, this standard defines the FL as the value of the stress range corresponding to 10^7 cycles.

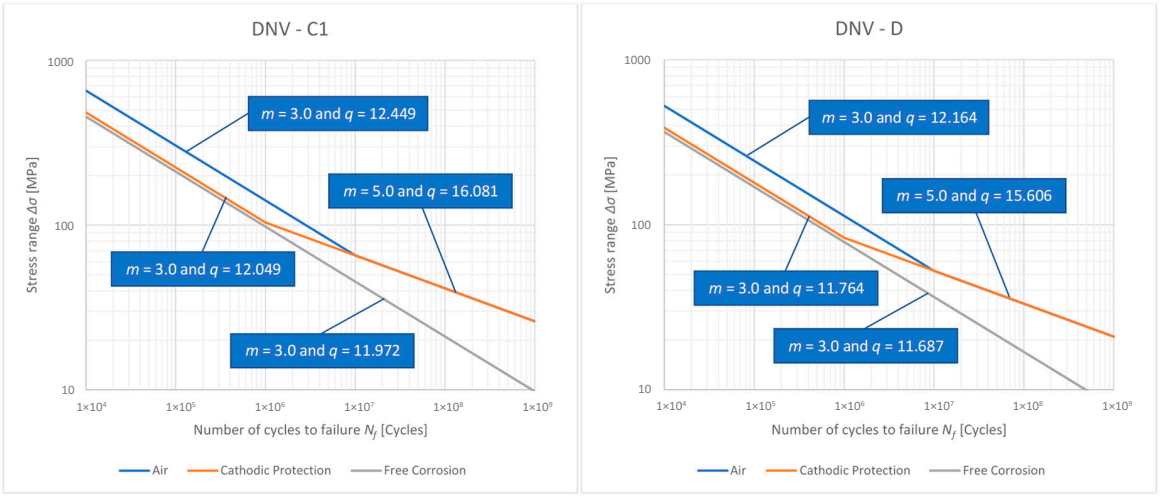

Figure 5. S-N curves recommended in the DNV standard for classes C1 (**left**) and D (**right**) in various environments.

In Figure 6, the S-N curves from BS for classes C and D are presented. Their main difference when compared to the DNV ones is the presence of a horizontal asymptote after 10^7 cycles in air and seawater with cathodic protection, as follows: the FL is set at 53 MPa for class D and 78 MPa for class C, while it is absent in seawater with free-corrosion conditions (as in DNV). The BS standard suggests a different number and location of changes in the inverse slope (CS) depending on the environment, as follows: in air, there is only one CS placed at 10^7 cycles; in seawater with cathodic protection, there are two CSs, with the additional one set at 144 MPa for class C and 84 MPa for class D; and, in seawater under free-corrosion conditions, no CSs are present. Among the three analyzed standards, BS is the only one in which some of these locations are given in MPa instead of the number of cycles. Another interesting consideration is that the recommended S-N curves for air and cathodic protection environments fall on top of each other in the UHCF regime.

Figure 7 illustrates the design curves in air for classes 112 and 90 of the EC standard. As reported in this figure, the fatigue design curves display two CSs, as follows: the first is placed at 5×10^6 cycles (where m switches from three to five), while the second is placed at 10^8 cycles. Eventually, there is a flat asymptote in the UHCF region from 10^8 cycles onwards, which, for classes 112 and 90, indicates FL values of 45 MPa and 36 MPa, respectively. As mentioned earlier, the EC standard does not provide any recommendations to account for the presence of seawater.

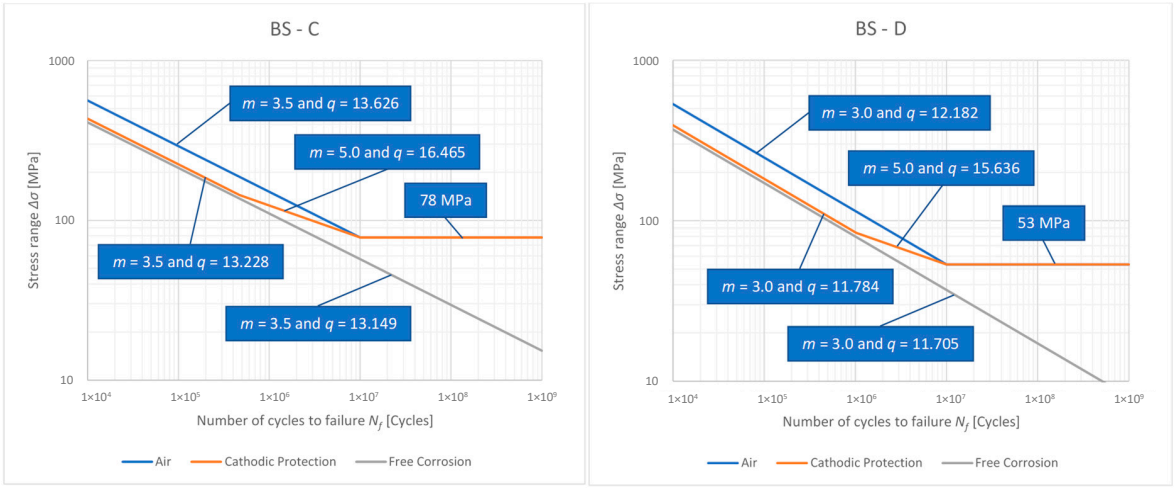

Figure 6. S-N curves from BS for classes C (**left**) and D (**right**) in various environments.

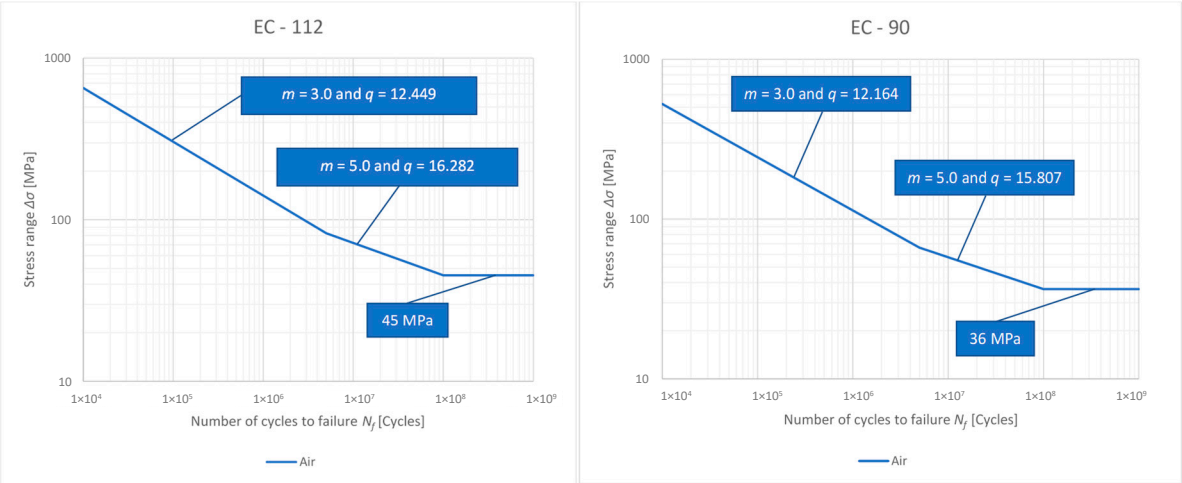

Figure 7. S-N curves from EC for classes 112 (**left**) and 90 (**right**) in air.

3.4. Comparison of S-N Fatigue Design Curves Depending on the Environment

This section presents a comparison of the fatigue design curves from the three different standards. The AW and GF classes are analyzed separately across the three environments of interest of this study (air, seawater with cathodic protection, and seawater with free corrosion). This results in six distinct plots.

In Figure 8, the S-N curves in air for classes C1, C, and 112 from the DNV, BS, and EC standards, respectively, are reported and compared with each other. In this configuration, it is worth highlighting the following observations: (i) DNV is the only design curve that does not display an FL by assuming that, under variable amplitude fatigue loading conditions, and in the absence of any stress risers at the weld toe, there is always a sufficient driving force to initiate the crack, even at very low stress range levels in the UHCF region; (ii) there is only one change in the inverse slope, which occurs at 10^7 cycles, according to both the DNV and BS standards, while the EC standard suggests two changes in the inverse slope at $5 \cdot 10^6$ and 10^8 cycles; (iii) the initial inverse slope of the S-N curve is $m = 3$, based on the DNV and EC recommendations, but $m = 3.5$ according to the BS standard; (iv) the flat asymptotes are placed at $N_f = 10^7$ and $N_f = 10^8$ according to BS and EC, respectively, with the latter being smaller in terms of MPa; and (v) the value of m after the first change in the inverse slope is $m = 5$, based on the DNV and EC standards. An overall comparison of the S-N fatigue design curves for the GF condition in air shows that, in the UHCF regime, the BS and DNV standards provide the least and the most conservative design curves, respectively, while the recommended design curve from the EC standard falls between these two.

The EC standard does not provide any information for the seawater environment. Instead, it states that the design curves in air can be used only under normal atmospheric conditions with adequate corrosion protection and maintenance. Therefore, only the DNV and BS standards are considered here to compare the S-N fatigue design curves in seawater.

In Figure 9, the S-N curves in seawater with cathodic protection from class C1 in DNV and class C in BS are presented. Among the different inverse slopes and intercepts, it is worthy to bring to the attention of the readers that the inverse slope of the initial part of the S-N curve, according to the BS standard, is 3.5, which is the same as the recommended value stated in the BS standard for the air environment. Another important observation when comparing these two S-N design curves is that, in the UHCF region, the BS standard suggests an FL (as it does in air), while the DNV standard employs a continuous inverse slope of five. Moreover, from the same figure, it can be seen that the fatigue design curve from DNV is characterized by one CS, while, in the BS standard, it is characterized by two. A final consideration about GF classes in seawater with cathodic protection is that, after 10^5 cycles, the DNV standard is more conservative than the BS one.

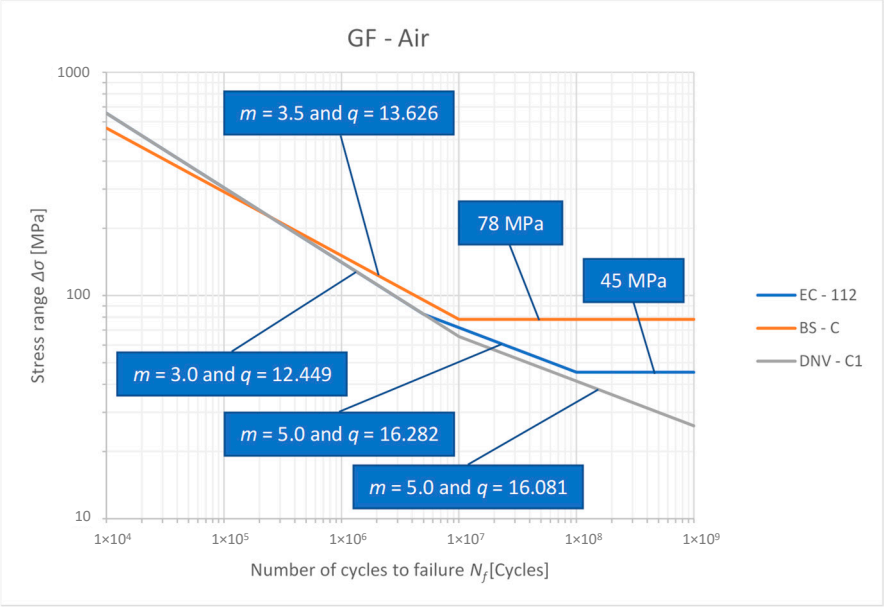

Figure 8. S-N curves comparison for classes C1, C, and 112 from DNV, BS, and EC, respectively, in air.

Following the comparison of the S-N curves in seawater with cathodic protection, a similar comparison has been made for the seawater environment with free-corrosion conditions (i.e., in the absence of cathodic protection), and the results are shown in Figure 10. As shown in this figure, the S-N curves from both standards display a similar trend, but with an inverse slope of 3 for class C1 in the DNV standard and 3.5 for class C in the BS one. In addition to that, unlike the S-N fatigue design curves in air and seawater with cathodic protection conditions, no change in the inverse slope is recommended by either of these two standards for both the HCF and the UHCF regions. This indicates that, when the welded structure is immersed in seawater without any cathodic protection, there will always be a sufficient driving force to initiate a crack, even at very low stress range levels. Last but not least, it can be observed that the recommended curve from the DNV standard is more conservative than that of the BS one after 10^5 cycles.

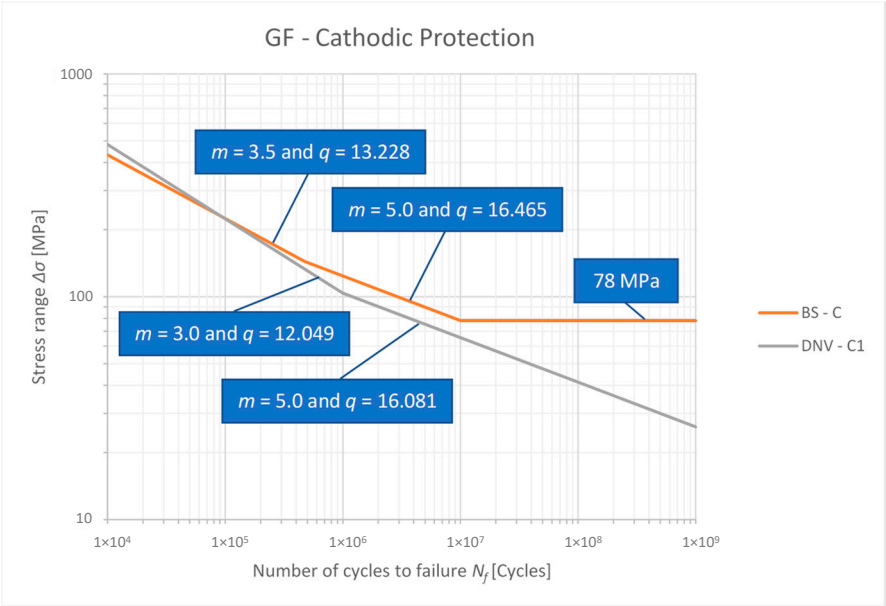

Figure 9. S-N curves comparison from DNV and BS for classes C1 and C, where the environment is seawater with cathodic protection.

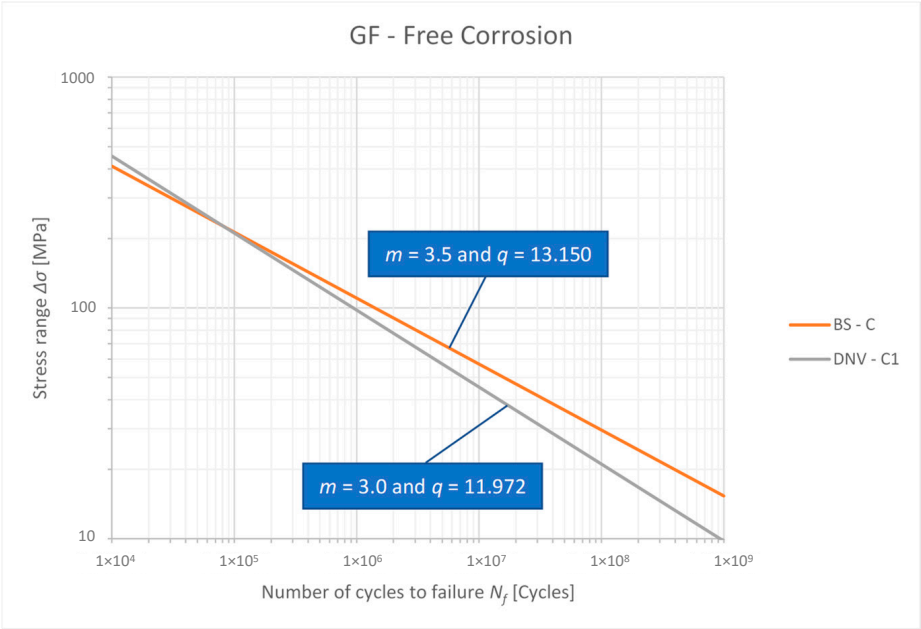

Figure 10. S-N curves comparison from DNV and BS for classes C1 and C, where the environment is seawater without cathodic protection.

The same comparison can be carried out for the AW curves, but the outcomes are almost the same. The only exception is that the inverse slope of the initial part of the S-N curve for the GF condition, according to class C in the BS standard, is 3.5, while this value is 3 for the AW condition, according to class D in the BS standard. In general, in the HCF regime, the AW curves are more similar to each other, compared to the GF condition. These features can be easily spotted by looking at Figure 11 or by comparing the inverse slopes and intercepts summarized in Tables 2–5.

Tables 2–5 systematically present all of the inverse slopes, intercepts, locations of changes in inverse slopes, and values of FL for all of the S-N fatigue design curves presented so far. The data are divided based on the GF and AW classes, as well as HCF and UHCF behaviors, to enhance the visual clarity and facilitate comprehension. If present, the first change in the inverse slope (1st CS) may indicate either the end of the HCF or the beginning of a horizontal FL asymptote. The locations of the 1st and 2nd CSs have been reported in terms of the number of cycles to failure in the tables below. The FL, if present, has to be intended as a horizontal plateau and is given in MPa. For the sake of comparison, some values have been calculated manually, since they were not directly provided in the standards, and are shown with a star sign (*). Since the EC standard does not contain any information about S-N curves in seawater with or without cathodic protection, the corresponding cells of the tables have been left blank.

Table 2. HCF data for ground flush welds (classes C1, C, and 112 according to DNV, BS, and EC, respectively). The calculated values have been marked with a star sign (*).

GF–HCF	**Air**			**Cathodic Protection**			**Free Corrosion**		
Standard	**DNV**	**BS**	**EC**	**DNV**	**BS**	**EC**	**DNV**	**BS**	**EC**
m	3.0	3.5	3.0	3.0	3.5	-	3.0	3.5	-
q	12.449	13.626 *	12.449 *	12.049	13.228 *	-	11.972	13.149 *	-
1st CS [Cycles]	10^7	10^7	5×10^6	10^6	4.72×10^5 *	-	-	-	-

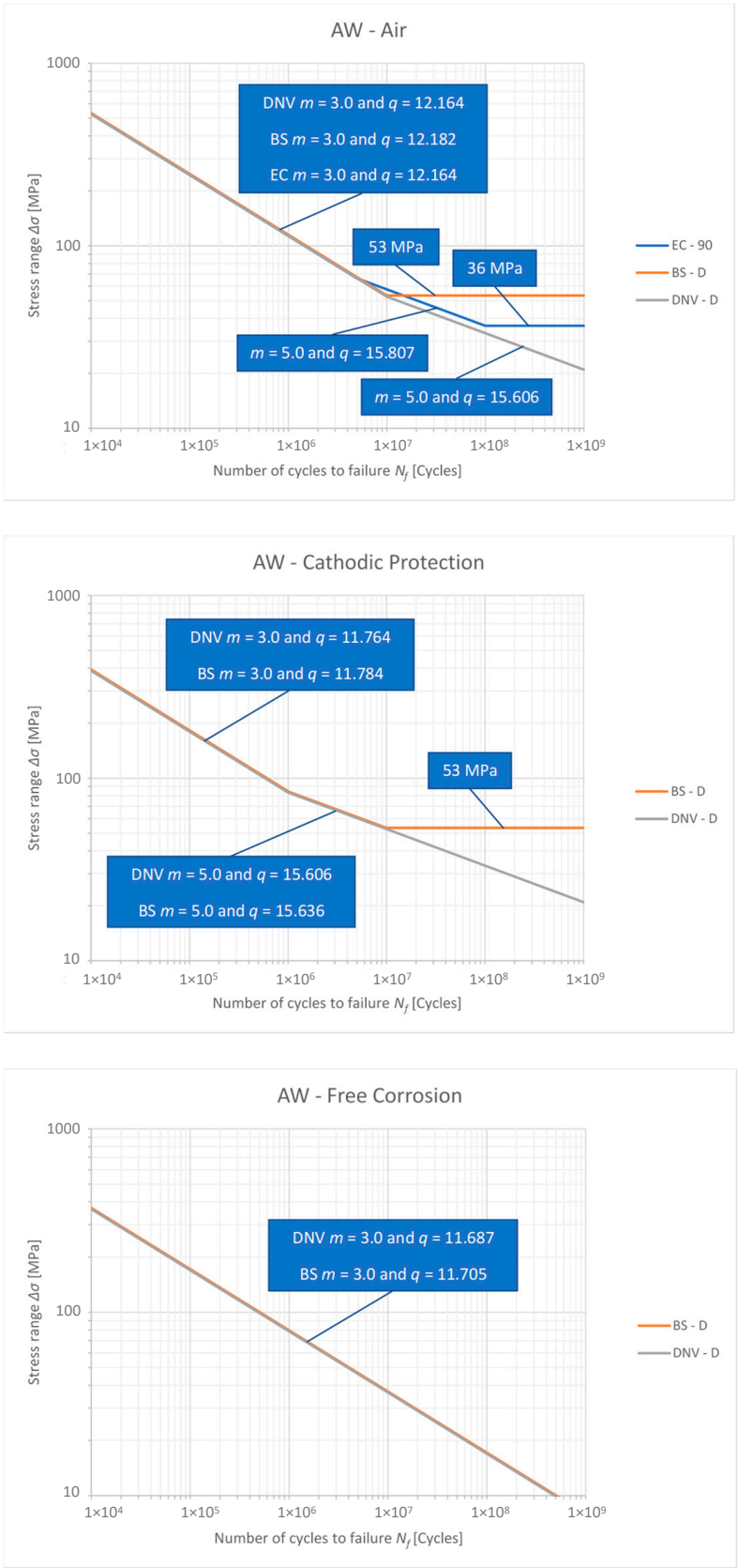

Figure 11. S-N curves comparison from DNV, BS, and EC for AW classes in air, seawater with cathodic protection, and seawater with free-corrosion conditions (from top to bottom, respectively).

Table 3. UHCF data for ground flush welds (classes C1, C, and 112 according to DNV, BS, and EC, respectively). The calculated values have been marked with a star sign (*).

GF–UHCF	Air			Cathodic Protection			Free Corrosion		
Standard	**DNV**	**BS**	**EC**	**DNV**	**BS**	**EC**	**DNV**	**BS**	**EC**
m	5.0	-	5.0	5.0	5.0	-	3.0	3.5	-
q	16.081	-	16.282 *	16.081	16.465 *	-	11.972	13.149 *	-
2nd CS [Cycles]	-	-	10^8	-	10^7	-	-	-	-
FL [MPa]	-	78	45*	-	78	-	-	-	-

Table 4. HCF data for as-welded conditions (class D according to DNV and BS, and class 90 according to EC). The calculated values have been marked with a star sign (*).

AW–HCF	Air			Cathodic Protection			Free Corrosion		
Standard	**DNV**	**BS**	**EC**	**DNV**	**BS**	**EC**	**DNV**	**BS**	**EC**
m	3.0	3.0	3.0	3.0	3.0	-	3.0	3.0	-
q	12.164	12.182 *	12.164 *	11.764	11.784 *	-	11.687	11.705 *	-
1st CS [Cycles]	10^7	10^7	5×10^6	10^6	1.03×10^6 *	-	-	-	-

Table 5. UHCF data for as-welded conditions (class D according to DNV and BS, and class 90 according to EC). The calculated values have been marked with a star sign (*).

AW–UHCF	Air			Cathodic Protection			Free Corrosion		
Standard	**DNV**	**BS**	**EC**	**DNV**	**BS**	**EC**	**DNV**	**BS**	**EC**
m	5.0	-	5.0	5.0	5.0	-	3.0	3.0	-
q	15.606	-	15.807 *	15.606	15.636 *	-	11.687	11.705 *	-
2nd CS [Cycles]	-	-	10^8	-	10^7	-	-	-	-
FL [MPa]	-	53	36 *	-	53	-	-	-	-

3.5. Fatigue Life Enhancement by Grinding the Weld Toe

Monopiles for offshore wind turbines are usually designed following the AW curves, rarely using the GF ones. In Table 6, the advantages of employing ground flush welds are reported in terms of the percentage increase in the number of cycles to failure for a given value of stress range. The reason for this beneficial effect can be mainly attributed to the weld toe removal, which eliminates the stress concentration factor. All of these values are reported as percentages and are calculated using (6), as follows:

$$life\ enhacement\ \% = \frac{N_{fGF} - N_{fAW}}{N_{fAW}} \times 100 = \left(10^{q_{GF} - m_{GF}\log\Delta\sigma - q_{AW} + m_{AW}\log\Delta\sigma} - 1\right) \times 100 \quad (6)$$

where N_{fGF} and N_{fAW}, q_{GF} and q_{AW}, and m_{GF} and m_{AW} are the number of cycles to failure, the intercepts, and the slopes corresponding to the GF and AW curves, respectively. As shown in Table 6, due to the power-law correlation between the stress range and the number of cycles to failure, the percentage of enhancement in fatigue life as a result of grinding the weld toe increases when decreasing the stress range level. Specifically, when $m_{GF} = m_{AW}$, this value depends only on the difference between the intercepts and not on the stress level. In fact, for DNV and EC, a value of 93% is achieved when $m = 3$ for both curves, and 199% when $m = 5$ for both curves. The percentage increase assumes the same values for both standards, because the difference in the intercept is very similar. Regarding BS, since the AW curve has a slope of 3 and the GF one has a slope of 3.5, the life enhancement

increases as the stress level decreases. This leads to very high values under free-corrosion conditions. When both N_{fA} and N_{fG} are equal to infinity, due to the presence of an FL, the cell is marked as 0% increase in fatigue life.

Table 6. The percentage increase in N_f when switching from AW curves to GF curves for all of the analyzed standards and environments.

AW to GF	**Air**			**Cathodic Protection**			**Free Corrosion**		
Standard	**DNV**	**BS**	**EC**	**DNV**	**BS**	**EC**	**DNV**	**BS**	**EC**
200 MPa	93%	97%	93%	93%	97%	-	93%	97%	-
50 MPa	199%	0%	199%	199%	0%	-	93%	294%	-
10 MPa	199%	0%	0%	199%	0%	-	93%	780%	-

Therefore, despite the associated costs for the grinding process, the GF condition generally offers to designers a wider fatigue life span than the AW one, depending on the stress range level and the environment. Due to their higher fatigue life, GF welds are preferable to design highly stressed welded links, the zone close to the flange, or at high-thickness changes.

3.6. Thickness Effect on Fatigue Life

According to the recommendations in the standards, all of the classes analyzed so far undergo a reduction in fatigue life due to the size effect only if the effective thickness t of the welded plates exceeds 25 mm. The effective thickness is equal to the actual thickness of the plates in BS and EC, and to the minimum value between $14 + 0.66l$ and the actual thickness of the plates in DNV (where l is the weld width, as reported in Figure 3).

To account for the thickness (or size) effect, the three codes agree on a correction factor k, defined in (7), as follows:

$$k = \left(\frac{t}{25}\right)^c \tag{7}$$

where t is the effective thickness in millimeters and c is a dimensionless exponent that depends on the standard chosen to design the monopile, on the class of the welded joint, and on the environment. The higher the values of these two parameters, the more pronounced the thickness effect. Factor k is a multiplier of the stress range in (1), such that a lower number of cycles to failure is obtained.

3.6.1. Role of the Weld Width on the Thickness Effect

In this section, the formula for the effective thickness present in DNV will be deepened. Thanks to some simple geometrical considerations, (8) correlates the weld width l with the actual thickness of the plates T and reveals the role of the former on the thickness effect.

$$l = 2(l_1 + l_2)\sin\frac{\alpha}{2} = 2\left(\frac{b}{2\sin\frac{\alpha}{2}} + \frac{2T}{3\cos\frac{\alpha}{2}}\right)\sin\frac{\alpha}{2} = b + \frac{4}{3}T\tan\frac{\alpha}{2} \tag{8}$$

In (8), b is the weld gap, l is the weld width, and α is the groove angle. All of these parameters are shown in Figure 12.

The asymmetric configuration has been chosen to obtain a higher value for the weld width. If a symmetric double-V groove is desired, the factor 4/3 in front of the thickness disappears. Setting $b = 3$ mm and $\alpha = 60°$ (values within the ranges suggested by ISO 9692-1:2013-12 [28] and aimed at increasing the value of l), the condition on the effective thickness present in DNV can be checked through the following inequality:

$$T > 14 + 0.66\left(b + \frac{4}{3}T\tan\frac{\alpha}{2}\right)$$

which leads to $T > 32.5$ mm. Thus, when $b = 3$ mm, $\alpha = 60°$, and $T > 32.5$ mm, the effective thickness can be expressed as show in (9), as follows:

$$t = 14 + 0.66\left(b + \frac{4}{3}T\tan\frac{\alpha}{2}\right) = 15.98 + 0.51T \quad (9)$$

The first consideration is that the higher the value of T, the lower the importance of b while evaluating the value of effective thickness. The second consideration is that, in DNV, the thickness effect is less impactful at very high values of T, with respect to the other two standards, because k is proportional to $0.51T$ instead of being proportional to T. In fact, as mentioned already, in BS and EC, the effective thickness always corresponds to the thickness of the plates ($t = T$). Moreover, it is worth pointing out that, if lower values of b and α are employed, both the threshold, which now is equal to 32.5 mm, and the coefficient in front of T, which now is equal to 0.51. become lower, leading to a less pronounced thickness effect. For instance, if $b = 1$ mm and $\alpha = 40°$, the threshold for the weld width to become the leading parameter for the evaluation of the thickness effect becomes $T > 21.57$ mm and the effective thickness is calculated through $t = 14.66 + 0.32T$.

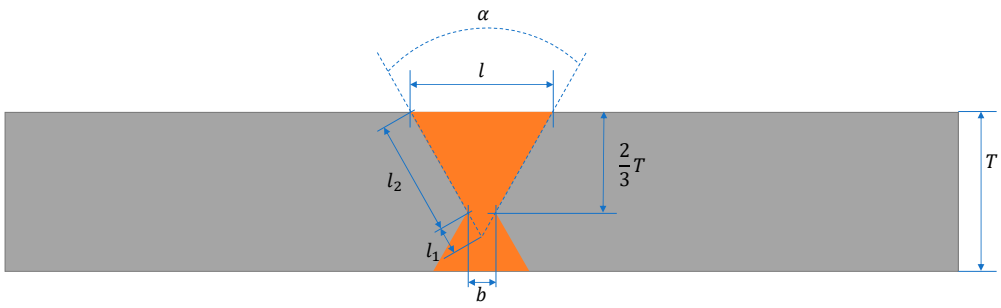

Figure 12. Welded joint showing geometrical parameters b (weld gap), l (weld width), α (groove angle), T (thickness of the plates), and other parameters useful to correlate the weld width with the thickness of the plates.

3.6.2. Comparison of the Thickness Correction Exponents

The value of the exponent c is always equal to 0.20, except for class C1 in the DNV standard, in which it is equal to 0.15 or 0.10, depending on the environment, and for class C in BS, in which the thickness correction is reported as not applicable (NA). All of the exponents are given in Table 7 for both GF and AW classes, depending on the environment. From this table, it appears that c depends only on the environment and the type of class (AW or GF); however, this is not the case for all standards. In fact, DNV is the only one that provides some kind of environmental sensitivity. Another interesting observation is that EC is the only standard that addresses the thickness effect in the same way for both GF and AW classes. Moreover, c does not depend on the number of cycles to failure in any of the standards, i.e., it does not bring any information to the thickness effect with regards to the HCF and UHCF regimes. Section 3.7 will explain how the standards address this aspect.

Table 7. Thickness correction exponents from DNV, BS, and EC for both GF and AW classes, depending on the environment.

c	**Air**			**Cathodic Protection**			**Free Corrosion**		
Standard	DNV	BS	EC	DNV	BS	EC	DNV	BS	EC
GF	0.10	NA	0.20	0.10	NA	-	0.15	NA	-
AW	0.20	0.20	0.20	0.20	0.20	-	0.20	0.20	-

3.6.3. S-N Curves for an Effective Thickness of 100 mm

In Figure 13, the S-N curves in air for GF classes with a thickness of $T = 100$ mm are reported. For DNV, an effective thickness of $t = 66.8$ mm has been calculated using $b = 3$ mm and $\alpha = 60°$. Under these conditions, for a number of cycles to failure lower than 1.6×10^8, EC is more conservative than DNV. Thus, at effective thickness values higher than 25 mm, the EC standard can be more conservative than DNV. Nevertheless, because of the absence of an FL, DNV will always be the most conservative standard in the UHCF regime. In the seawater environment (with or without cathodic protection), the reciprocal distance between the S-N curves for classes C from BS, which is not affected by a thickness correction, and C1 from DNV increases with the thickness. Hence, DNV curves are more conservative than the BS ones in all environments. By comparing Figures 8 and 13 it can be seen that the reciprocal distances between the S-N curves change consistently. This happens because, for GF welds, as the thickness of the welded joint increases, curve C in the BS remains unchanged, while the other two curves shift downwards by different factors. Specifically, the DNV curve is less affected by the thickness effect compared to the EC one because of both the lower thickness correction exponent and the different formula for the effective thickness.

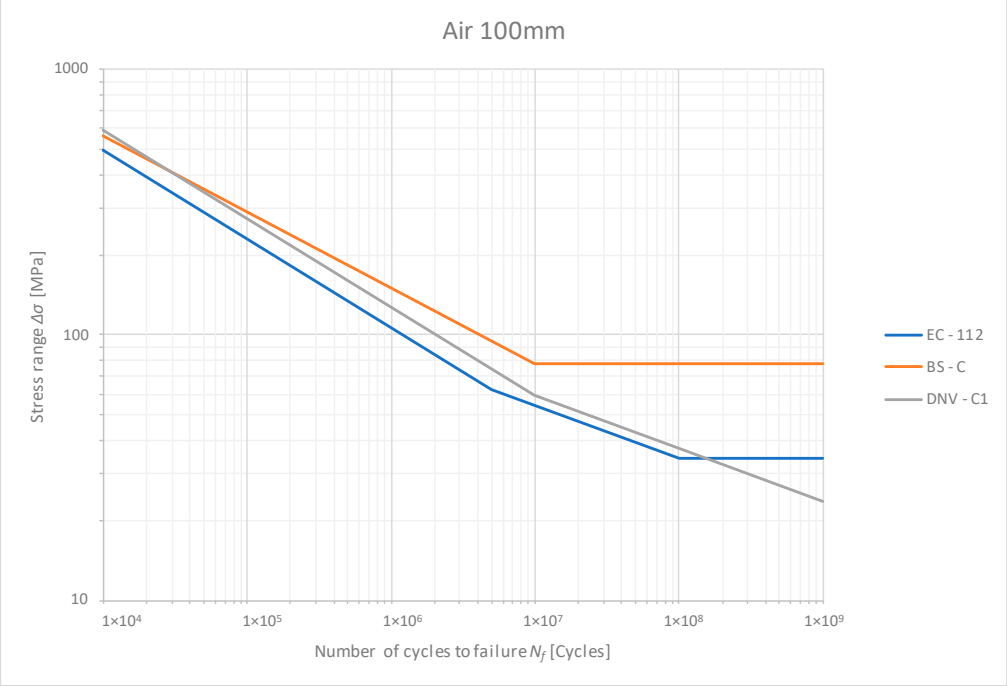

Figure 13. S-N curves comparison for classes C1, C, and 112 from DNV, BS, and EC, respectively, where the environment is air and the thickness is 100 mm.

As regards the AW classes, since BS and EC share the same exponent in all environments, their S-N curves at thickness values higher than 25 mm will be shifted down by the same factor. The DNV ones, instead, will be less affected by the thickness effect, because of the different formula for the effective thickness. However, they will be more conservative in the UHCF, due to the absence of an FL.

3.7. Combined Detrimental Effect of Increase in Thickness and UHCF

Interesting considerations in regard to the percentage decrease in the number of cycles to failure when increasing the thickness can also be carried out. Table 8 reports the percentage decrease in the number of cycles to failure when the thickness T increases from

25 mm to 100 mm for some selected stress ranges. The data are given for all of the analyzed standards and environments and were calculated using (10), as follows:

$$Change\ in\ life\ \% = \frac{N_{f100} - N_{f25}}{N_{f25}} \times 100 \quad (10)$$

where N_{f100} and N_{f25} are the number of cycles to failure corresponding to the 100 mm and 25 mm curves, respectively. Once again, the values of the geometrical parameters of the welded joint that have been used to calculate the effective thickness for the DNV curves are $b = 3$ mm and $\alpha = 60°$. It can be seen that the reduction in fatigue life increases when decreasing the stress range (i.e., in the UHCF regime). Additionally, because of the thickness increase, the location of the CS might shift down to a lower stress value. Hence, with the same stress range, the inverse slope and intercept may vary when calculating N_f at 25 mm or 100 mm. This is the case for class D of DNV in air conditions at $\Delta\sigma = 50$ MPa, where, for $T = 25$ mm, the first CS is at 53 MPa, but, for $T = 100$ mm, it goes down to 43 MPa. In all of the other cases, when the slope and the intercept do not change and a thickness of $T = 100$ mm is used, the reduction in the number of cycles to failure can be calculated using (11). This time, the factor of 100 to obtain the percentage has been omitted for a neater representation.

$$Change\ in\ life = k^{-m} - 1 = \left(\frac{t}{25}\right)^{-c \cdot m} - 1 \quad (11)$$

From this equation it can be seen that the highest reductions in fatigue life are achieved when c and m are at maximum, i.e., for $c = 0.2$ (very pronounced thickness effect, such as in AW classes) and $m = 5$ (UHCF regime).

Table 8. The percentage decrease in N_f when thickness increases from 25 mm to 100 mm for all of the analyzed standards and environments.

GF	**Air**			**Cathodic Protection**			**Free Corrosion**		
Standard	**DNV**	**BS**	**EC**	**DNV**	**BS**	**EC**	**DNV**	**BS**	**EC**
200 MPa	−25%	0%	−56%	−25%	0%	-	−36%	0%	-
50 MPa	−39%	0%	−75%	−39%	0%	-	−36%	0%	-
10 MPa	−39%	0%	0%	−39%	0%	-	−36%	0%	-
AW	Air			Cathodic Protection			Free Corrosion		
Standard	DNV	BS	EC	DNV	BS	EC	DNV	BS	EC
200 MPa	−45%	−56%	−56%	−45%	−56%	-	−45%	−56%	-
50 MPa	−50%	−inf	−75%	−63%	−inf	-	−45%	−56%	-
10 MPa	−63%	0%	0%	−63%	0%	-	−45%	−56%	-

4. Discussion

4.1. Experimental Data and S-N Parameters

First, it is worth discussing the experimental data used to derive the S-N curves currently available in the standards. From a historical point of view, design practices find their roots in the oil and gas industry. Databases that are over 30 years old and inherent to components with different applications are currently employed to suggest how to design against fatigue in very-large-scale offshore wind turbine structures like monopiles [24,26]. The tests conducted to establish the S-N curves were primarily performed in the HCF region, due to the time-consuming nature of fatigue testing and the lack of reliable high-frequency testing facilities [10–12]. Furthermore, due to the complexity of carrying out large-scale specimen tests, the data refer to cyclic failures of relatively thin samples [26]. In

this regard, DNV is the only standard that explicitly reports that its S-N curves are designed to assess fatigue lives in the HCF regime.

For fatigue design in seawater environments with and without cathodic protection, the corresponding S-N curves from DNV and BS can be observed to scale by factors of 2.5 and 3.0, respectively, from the air environment. For free-corrosion conditions, this life reduction factor has been justified by observing the decrease in the fatigue lives of some specimens tested in air in the HCF regime [24,29]. In addition, as stated in one of the previous sections, corrosion fatigue is a frequency-dependent phenomenon. This means that, under this condition, one slope and one intercept are not able to thoroughly describe the fatigue behavior of a material. Thus, one more experimental parameter is needed in order to give a clearer representation of the design curves for the free-corrosion conditions, perhaps the frequency employed during the tests.

In the SLIC Joint Industry Project, a recent inter-laboratory test program, fatigue specimens were extracted from 50 mm thick welded steel plates manufactured using a process identical to that employed in the offshore wind industry and prepared under both GF and AW conditions [30]. The number of cycles to failure of the specimens ranges from 10^4 to 5.36×10^6 cycles. Mehmanparast et al. utilized these tests to determine new values for the slope and intercept of the S-N curves of AW classes in air [26]. The authors derived the following four linear models: linear regression fixing $m = 3$, linear regression without fixing the inverse slope, Bayesian regression fixing $m = 3$, and Bayesian regression without fixing the inverse slope. Two additional Bayesian regression models accounting for run-outs were calculated but were excluded here for a better comparison with the design curves of the standards. Table 9 compares the slopes, intercepts, standard deviations (SD), and number of cycles to failure at 200 and 80 MPa of these four models with the corresponding parameters from the standards under investigation. All of the parameters in the table are based on the mean curve minus two standard deviations, and the number of cycles to failure at 200 and 80 MPa for the three standards were calculated using the thickness correction factor $k(T = 50 \text{ mm}, c = 0.2)$. Again, for DNV, standard values of $b = 3$ mm and $\alpha = 60^\circ$ have been used. Lastly, q values for DNV, BS, and EC have been adapted to include the thickness correction factor, thus facilitating the comparison with the models provided by Mehmanparast et al. Moreover, Table 10 shows the percentage increase or decrease in the number of cycles to failure when comparing the values calculated from the four models with those from DNV.

First, it is necessary to point out that the difference between the standard deviations can be considered acceptable. Then, it is important to highlight the difference in terms of the number of cycles to failure between the four models and the standards. Fixed slope models (i.e., linear fixed and Bayesian fixed) are more conservative than the standards independently of the selected stress range (at $\Delta\sigma < 80$ MPa standards display flat asymptotes or inverse slopes of five, so even higher values for N_f are predicted compared to the linear fixed and Bayesian fixed ones). As regards linear unfixed, Figure 14 shows the percentage increase or decrease in the number of cycles to failure when comparing DNV values (N_{fDNV}) with the linear unfixed ones (N_{fLU}). Neglecting the factor of 100, the percentage variation has been calculated using (12). The latter is valid until DNV changes in inverse slope (i.e., $N_{fDNV} \leq 10^7$).

$$\frac{N_{fLU} - N_{fDNV}}{N_{fDNV}} = 10^{12.786 - 12.033 \frac{3.37}{3}} N_{fDNV}^{\frac{0.37}{3}} - 1 \tag{12}$$

Figure 14 is not in log–log coordinates in order to emphasize the percentage variation between 10^6 and 10^7 cycles. It is straightforward to see that the higher the number of cycles to failure, the higher the percentage increase. Specifically, at around $5 \cdot 10^6$, the fatigue life predicted by the linear unfixed model is more than 25% higher than that of the DNV one. Figure 15 shows the S-N curves of the AW classes from the standards in air for a thickness of $T = 50$ mm and the linear unfixed model, as follows: the solid line is the mean curve (LU-m), while the dashed line represents the linear unfixed model, as depicted in Table 9

(i.e., the mean curve minus two standard deviations, LU-2SD). While looking at Figure 15, it is important to remember that the fit lines come from experiments carried out up to 5.36×10^6 cycles.

Since the Bayesian unfixed model has similar slope and intercept compared to the linear unfixed one, the same considerations can be used.

Thus, the key concept from this analysis is that there are real-scale experimental data suggesting that the slope of three and the thickness correction might need to be revised when applied to monopile design [26].

Table 9. Slopes, intercepts, standard deviations, and number of cycles to failure at 200 and 80 MPa for the four models developed by Mehmanparast et al. and the three standards under investigation.

	Linear Fixed	**Linear Unfixed**	**Bayesian Fixed**	**Bayesian Unfixed**	**DNV**	**BS**	**EC**
m	3.00	3.37	3.00	3.36	3.0	3.0	3.0
q	11.953	12.786	11.940	12.765	12.033	12.001	11.983
SD	0.21	0.21	0.22	0.22	0.200	0.2095	NP
N_f at 200 MPa	1.12×10^5	1.08×10^5	1.09×10^5	1.08×10^5	1.35×10^5	1.25×10^5	1.20×10^5
N_f at 80 MPa	1.75×10^6	2.36×10^6	1.70×10^6	2.35×10^6	2.11×10^6	1.96×10^6	1.88×10^6

Table 10. The percentage increase or decrease in the number of cycles to failure at 200 and 80 MPa calculated by comparing the results obtained from the four models developed by Mehmanparast et al. with those from DNV.

	Linear Fixed	**Linear Unfixed**	**Bayesian Fixed**	**Bayesian Unfixed**
Change in N_f at 200 MPa	−17%	−20%	−19%	−20%
Change in N_f at 80 MPa	−17%	12%	−19%	11%

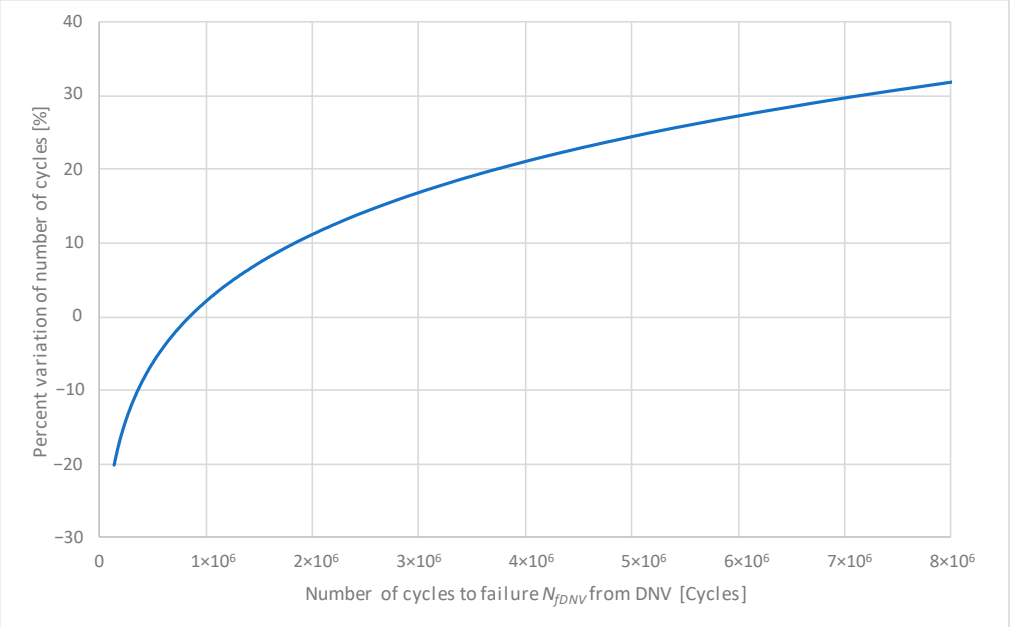

Figure 14. The percentage variation of number of cycles to failure between DNV and linear unfixed in air for class D.

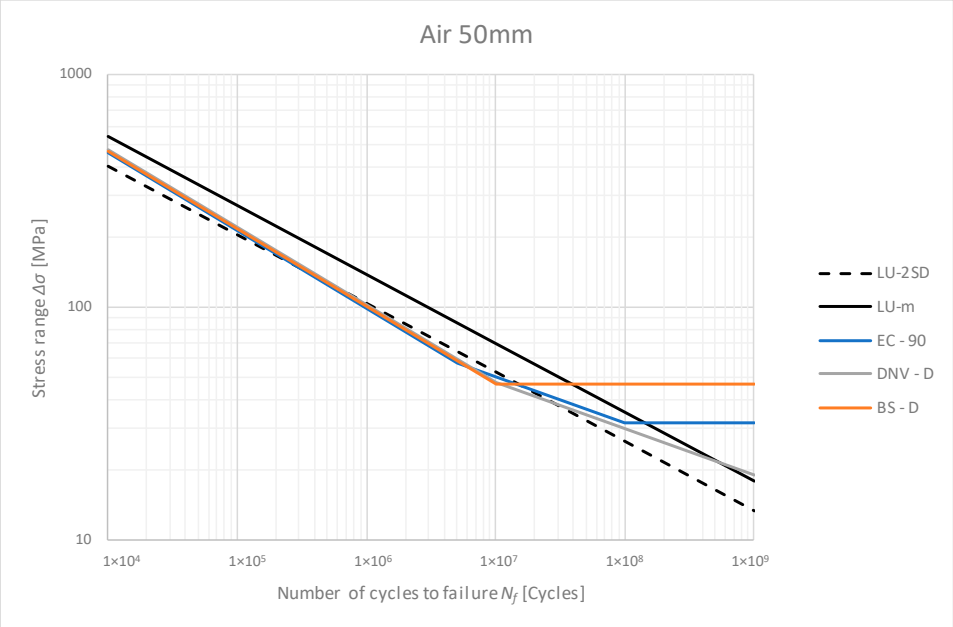

Figure 15. Comparison between the S-N curves coming from the standards and the linear unfixed model by Mehmanparast et al. in air with a thickness of 50 mm for AW classes.

4.2. Ultrahigh-Cycle Fatigue

The UHCF regime is the zone in which the majority of the differences between the standards arise. For a number of cycles high enough, regardless of the thickness, DNV is always the most conservative, mainly because of the complete absence of horizontal fatigue endurance limit asymptotes. However, it is important to remember that no significant UHCF data, particularly on high-thickness welded samples, have been used to develop these curves. Hence, whether a horizontal asymptote can be drawn or not and the exact slope of the S-N curves in the UHCF region are some things that need to be addressed in future works. The same considerations can be taken for the locations and the amount of CS.

After a long exposure to cyclic loadings, both DNV and BS predict an overlap between their air and cathodic protection curves. This feature has already been investigated [24], but further clarifications might be useful to assess, for example, the role of erosion in the presence of a sandy seabed.

4.3. Thickness Effect

The thickness effect on the fatigue life of structures has been well known for decades, but, due to its complexity, it is usually addressed using empirical correction factors [10–12,25,31]. Consequently, some studies have investigated their potential over-conservativeness. It has been found that, for axially loaded butt joints, this effect might be less pronounced than that seen in other types of joints, suggesting the use of lower values for k [32]. First, is important to distinguish between the thickness effect on AW and GF components, as follows: as a consequence of what has been said so far, the former is more likely to have a major contribution from the geometric effect (ratio ρ/t), while the latter from the weakest link concept. Since the underlying mechanism is different for the two types of classes, it appears sensible to employ different correction factors. This is performed in DNV by modifying the exponent c, and in BS by removing any correction factor for class C. On the contrary, in EC, there is no difference in terms of the thickness correction factor between the two types of classes. The standards do not agree on a common value for the exponent c of GF classes; moreover, for this type of weld, the influence of the thickness on the fatigue strength is affected by high scatter [33]. Hence, other tests at high thickness values must be carried out in the future to obtain a more reliable correction factor k for GF classes. An idea to differentiate between the two mechanisms might be to keep the

current thickness correction formula for the AW classes, while using a different one for the GF classes. An idea for the latter could be to make it depend on the volume of the weld seam (either including the HAZ or not) to account for the weak places within it.

As regards the environmental component of the thickness effect, class C1 from DNV is the only one in which the thickness correction is environment-sensitive, specifically through the exponent c. All of the other classes from the other two standards do not consider this feature. Further investigations will be needed, since there are not enough data available [34].

The thickness affects the fatigue behavior of welded joints in the HCF and UHCF regimes in different ways. In fact, as reported above when describing Table 8 and (11), fatigue lives calculated at effective thickness values higher than 25 mm are UHCF-sensitive through m. In particular, UHCF is designed as a detrimental factor for the fatigue life of thick welded joints. This can be explained by the fact that, in this region, cracks usually originate in the bulk, and, since these details can be reasonably considered two dimensional, an increase in thickness causes a sensible and negligible increase in volume and surface area, respectively. Thus, more sites for crack initiation are available. Moreover, in the UHCF regime, the higher the thickness, the more likely it is for a crack to nucleate far from the surface. This can be the case for GF components, while, for the AW ones, a deeper analysis should be carried out because of the stress intensity factor present at the weld toe.

4.4. Future Developments

From this work, the following questions arise: (i) Do S355 double-V transverse butt welds have a flat asymptote in the UHCF region? If not, what should be the slope of their corresponding S-N curves? (ii) In the UHCF regime, do the data in air condition overlap with the cathodic protection condition? (iii) Is a reduction factor of 3 correct to account for free-corrosion conditions (and similarly, 2.5 for cathodic protection)? (iv) Is the exponent c affected by the environment? (v) Increasing the number of CSs helps to better fit data, but how many are needed and where is best to place them? (vi) Is there any detrimental synergy between the thickness effect and the UHCF regime? If so, is it correct to account for it by means of the coefficient m, as described in Section 3.7? (vii) When UHCF and corrosion are present at the same time, how does the fatigue behavior change? Since corrosion is a surface phenomenon, if UHCF failures for GF welds still take place in the bulk, can the effect of the two be unbounded? (viii) Are the current S-N curves representative for monopile design? (ix) Is it correct to mitigate the thickness effect at high thickness values by introducing the weld width in the thickness correction factor, as DNV does? (x) All three of the analyzed standards deal with the influence played by the thickness effect on the GF classes in different ways, thus, further clarifications are needed.

5. Conclusions

In this work, the fatigue behavior of double-V transverse butt welds has been studied, as proposed by DNV, BS, and EC. As a result of the analysis of these three standards, DNV has consistently been found to be the most conservative in the UHCF regime, regardless of the thickness effect and the environment, primarily due to the lack of a flat asymptote in its C1 and D curves. On the contrary, S-N curves from both BS and EC display a fatigue limit, with the latter of the two also having more than one CS. The comparisons show that the differences between the design curves in air conditions amplify over 10 million cycles, due to different slope change-over points recommended in various standards. As regards the thickness effect, it is considered negligible for class C from BS, and it is described by the same factor for both class 112 and 90 from EC. DNV is the only standard that specifies an environment-sensitive thickness correction. Moreover, it has been observed that, in this standard, the thickness effect is less pronounced for very high thickness values, due to the inclusion of the weld width in the calculations (see Section 3.6.1). Also, it has been shown that the highest reduction in fatigue life has been found for thick AW joints in the UHCF regime. Under these conditions, when a thickness of 100 mm is considered,

the allowable fatigue life can drop by up to 75% (see Table 8). Within the context of the environmental effect on the fatigue behavior of welded joints, the analysis narrowed to DNV and BS because EC does not provide any recommendations for seawater. In the HCF regime, free-corrosion conditions have been obtained by scaling the data in air conditions by a factor of three. Similarly, under cathodic protection, a factor of 2.5 has been used. Additionally, it has been observed that scarce information is provided with regards to the frequency range for which these corrosion fatigue design curves are valid. The S-N curves in the standards were obtained from thin specimens in the HCF regime, and there are real-scale experiments suggesting that the slope of three might be overconservative when it comes to monopile design [26]. Thus, further investigations are needed to improve the fatigue design in this sector by reducing the level of conservatism for the longer operation of offshore wind turbine assets.

Author Contributions: Conceptualization, F.D.S. and A.M.; methodology, F.D.S.; formal analysis, F.D.S.; investigation, F.D.S. and G.Z.; writing—original draft preparation, F.D.S.; writing—review and editing, A.M. and G.Z.; supervision, A.M.; funding acquisition, A.M. All authors have read and agreed to the published version of the manuscript.

Funding: Federico Della Santa would like to thank EPSRC to support his doctoral studies through the DTP funding scheme.

Institutional Review Board Statement: Not applicable.

Informed Consent Statement: Not applicable.

Data Availability Statement: The data will be made available upon request.

Conflicts of Interest: Author Gianluca Zorzi was employed by the company RWE Offshore Wind GmbH. The remaining authors declare that the research was conducted in the absence of any commercial or financial relationships that could be construed as a potential conflict of interest.

References

1. International Renewable Energy Agency (IRENA). Tripling Renewable Power and Doubling Energy Efficiency by 2030: Crucial Steps towards 1.5 °C. 2023. [Online]. Available online: https://www.irena.org/Publications/2023/Oct/Tripling-renewable-power-and-doubling-energy-efficiency-by-2030 (accessed on 22 January 2024).
2. Leite, O.B. Review of Design Procedures for Monopile Offshore Wind Structures. Universidade do Porto, Porto, 2015. [Online]. Available online: https://www.slideshare.net/slideshow/review-of-design-procedures-for-monopile-offshore-wind-structures/54025518 (accessed on 17 January 2024).
3. Musial, W.; Spitsen, P.; Duffy, P.; Beiter, P.; Shields, M.; Mulas Hernando, D.; Hammond, R.; Marquis, M.; King, J.; Sathish, S. *Offshore Wind Market Report: 2023 Edition*; Department of Energy: Washington, DC, USA, 2023.
4. Nordenham, S. Steelwind Nordenham Company Brochure. Nordenham. 2021. [Online]. Available online: https://www.steelwind-nordenham.de/steelwind/index.shtml.en (accessed on 21 May 2024).
5. Jacob, A.; Oliveira, J.; Mehmanparast, A.; Hosseinzadeh, F.; Kelleher, J.; Berto, F. Residual stress measurements in offshore wind monopile weldments using neutron diffraction technique and contour method. *Theor. Appl. Fract. Mech.* **2018**, *96*, 418–427. [CrossRef]
6. Haagensen, P.J. Fatigue strength improvement methods. In *Fracture and Fatigue of Welded Joints and Structures*; Macdonald, K.A., Ed.; Woodhead Publishing Limited: Cambridge, UK, 2011; Chapter 11; pp. 297–329. [CrossRef]
7. Dowling, N.E. *Mechanical Behavior of Materials*, 4th ed.; Pearson: Harlow, UK, 2013.
8. Murakami, Y. (Ed.) Stress concentration. In *Metal Fatigue*, 2nd ed.; Elsevier: Amsterdam, The Netherlands, 2019; Chapter 2; pp. 13–27. [CrossRef]
9. Inglis, C.E. Stress in a plate due to the presence of cracks and sharp corners. *Trans. Inst. Nav. Archit.* **1913**, *55*, 219–241.
10. *DNV-RP-C203-2021*; Fatigue Design of Offshore Steel Structures. Det Norske Veritas (DNV): Bærum, Norway, 2021.
11. *BS 7608:2014+A1:2015*; Guide to Fatigue Design and Assessment of Steel Products. BSI Standards Limited: London, UK, 2015.
12. *EN 1993-1-9*; Eurocode 3: Design of Steel Structures—Part 1–9: Fatigue. The European Union: Brussels, Belgium, 2005.
13. Mughrabi, H. On 'multi-stage' fatigue life diagrams and the relevant life-controlling mechanisms in ultrahigh-cycle fatigue. *Fatigue Fract. Eng. Mater. Struct.* **2002**, *25*, 755–764. [CrossRef]
14. Schaumann, P.; Steppeler, S. Fatigue tests of axially loaded butt welds up to very high cycles. In *Procedia Engineering*; Elsevier Ltd.: Amsterdam, The Netherlands, 2013; pp. 88–97. [CrossRef]
15. England, A.; Toumpis, A.; Gorash, Y. Very High Cycle Fatigue of Welds: A Review. *Metals* **2023**, *13*, 1860. [CrossRef]

16. Mehmanparast, A.; Vidament, A. An accelerated corrosion-fatigue testing methodology for offshore wind applications. *Eng. Struct.* **2021**, *240*, 112414. [CrossRef]
17. Xiong, J.J.; Shenoi, R.A. *Fatigue and Fracture Reliability Engineering*; Springer Series in Reliability Engineering; Springer: London, UK, 2011. [CrossRef]
18. Bathias, C. There is no infinite fatigue life in metallic materials. *Fatigue Fract. Eng. Mater. Struct.* **1999**, *22*, 559–565. [CrossRef]
19. Sakai, T.; Sato, Y.; Nagano, Y.; Takeda, M.; Oguma, N. Effect of stress ratio on long life fatigue behavior of high carbon chromium bearing steel under axial loading. *Int. J. Fatigue* **2006**, *28*, 1547–1554. [CrossRef]
20. Pyttel, B.; Schwerdt, D.; Berger, C. Very high cycle fatigue—Is there a fatigue limit? *Int. J. Fatigue* **2011**, *33*, 49–58. [CrossRef]
21. Weibull, W. The Phenomenon of Rupture in Solids. *Ingeniörs Vetensk. Akad.* **1939**, *153*, 1–55.
22. Weibull, W. A Statistical Theory of the Strength of Materials. *Ingeniörs Vetensk. Akad.* **1939**, *151*, 1–45.
23. Weibull, W. A Statistical Distribution Function of Wide Applicability. *J. Appl. Mech.* **1951**, *18*, 293–297. [CrossRef]
24. Brennan, F.; Tavares, I. Fatigue design of offshore steel mono-pile wind substructures. *Proc. Inst. Civ. Eng. Energy* **2014**, *167*, 196–202. [CrossRef]
25. Berge, S. On the effect of plate thickness in fatigue of welds. *Eng. Fract. Mech.* **1985**, *21*, 423–435. [CrossRef]
26. Mehmanparast, A.; Chahardehi, A.; Brennan, F.; Manzocchi, M. Re-evaluation of fatigue design curves for offshore wind monopile foundations using thick as-welded test specimens. *Eng. Fail. Anal.* **2024**, *158*, 107971. [CrossRef]
27. Arany, L.; Bhattacharya, S.; Macdonald, J.; Hogan, S.J. Design of monopiles for offshore wind turbines in 10 steps. *Soil Dyn. Earthq. Eng.* **2017**, *92*, 126–152. [CrossRef]
28. *ISO 9692-1:2013-12*; Welding and Allied Processes—Types of Joint Preparation. International Organization for Standardization (ISO): Geneva, Switzerland, 2013.
29. Maddox, S.J. International efforts on fatigue of welded constructions. A review of Commission XIII activities. *Weld. World* **1993**, *31*, 86–92.
30. Structural Lifecycle Industry Collaboration (SLIC), S-N Curves and Guidance for Fatigue Assessment of Butt Welded Thick Steel Plates Based on Large Scale Tests. Marine Data Exchange, 2019. [Online]. Available online: https://www.marinedataexchange.co.uk/details/2115/packages (accessed on 4 March 2024).
31. Lee, Y.-L.; Pan, J.; Hathaway, R.B.; Barkey, M.E. *Fatigue Testing and Analysis (Theory and Practice)*; Elsevier: Amsterdam, The Netherlands, 2005.
32. Pedersen, M.M. Thickness Effect in Fatigue of Welded Butt Joints: A Review of Experimental Works. *Int. J. Steel Struct.* **2019**, *19*, 1930–1938. [CrossRef]
33. Braun, M.; Baumgartner, J.; Hofmann, G.; Drebenstedt, K.; Bauer, N.M.; Bakhschi, H.; Kuhlmann, U. A statistical assessment of the fatigue strength improvement of butt-welded joints by flush grinding. *Weld. World* **2023**, *67*, 2345–2359. [CrossRef]
34. Zhao, W.; Hsu, W.T. Re-evaluation of fatigue thickness effect based on fatigue test database. *J. Mar. Sci. Eng.* **2020**, *8*, 895. [CrossRef]